Supporting Information

Finley et al. 10.1073/pnas.1115813109

SI Materials and Methods

Metabolite Profiling. Serum was harvested by cardiac puncture at sacrifice. Three separate liquid chromatography (LC)/MS methods were used to profile metabolites in each plasma sample: (*i*) a hydrophobic interaction liquid chromatography (HILIC) method for the analysis of polar metabolites in the positive ion mode, (*ii*) an amine modified HILIC method to measure polar metabolites in the negative ion mode, and (*iii*) a reverse phase (RP) method to profile lipids. LC/MS analyses were performed using the following instrumentation, respectively: a 4000 Qtrap triple quadrupole mass spectrometer (AB Sciex) coupled to a 1100 Series pump (Agilent Technologies) and an HTS PAL autosampler (Leap Technologies), a 5500 Qtrap triple quadrupole mass spectrometer (AB Sciex) coupled to an Acquity ultra performance liquid chromatography (UPLC) (Waters), and a Qstar-XL quadrupole–time-of-flight (TOF) mass spectrometer coupled to a 1100 Series pump and autosampler (Agilent Technologies). For each HILIC method, MS analyses were carried out using electrospray ionization and selective multiple reaction monitoring scans in the respective ion mode. Declustering potentials and collision energies were optimized for each metabolite by infusion of reference standards before sample analyses. For HILIC analyses in the positive mode, plasma samples (10 μL) were prepared via protein precipitation with the addition of nine volumes of 74.9:24.9:0.2 vol/vol/v acetonitrile/methanol/formic acid containing stable isotope-labeled internal standards (valine-d8; Isotec and phenylalanine-d8; Cambridge Isotope Laboratories). The samples were centrifuged (10 min, 8,220 × *g*, 4 °C), and the supernatants were injected directly onto a 150 × 2.1 mm Atlantis HILIC column (Waters). The column was eluted isocratically at a flow rate of 250 μL/min with 5% mobile phase A (10 mM ammonium formate and 0.1% formic acid in water) for 1 min followed by a linear gradient to 40% mobile phase B (acetonitrile with 0.1% formic acid) over 10 min. The ion spray voltage was 4.5 kV and the source temperature was 450 °C. For HILIC analyses in the negative mode, plasma samples (30 μL) were extracted with the addition of four volumes of 80% methanol containing inosine-15N4, thymine-d4, and glycocholate-d4 (Cambridge Isotope Laboratories). The metabolites were eluted with a linear gradient using a 150 × 2.0 mm Luna NH2 column (Phenomenex) at a flow rate of 400 μL/min initially with 10% mobile phase A (20 mM ammonium acetate and 20 mM ammonium hydroxide in water) to 0% mobile phase B (10 mM ammonium hydroxide in 75:25 vol/vol acetonitrile/methanol) for 10 min and maintained isocratically for 2 min. The ion spray voltage was −4.5 kV and the source temperature was 500 °C. Plasma samples (10 μL) were extracted for lipid analyses with 190 μL of isopropanol containing 1-dodecanoyl-2-tridecanoyl-sn-glycero-3-phosphocholine (Avanti Polar Lipids). After centrifugation, supernatants were injected directly onto a 150 × 3.0 mm Prosphere HP C4 column (Grace). The column was eluted isocratically at a flow rate of 350 μL/min with 80% mobile phase A (95:5:0.1 vol/vol/v 10 mM ammonium acetate/methanol/acetic acid) for 2 min followed by a linear gradient to 80% mobile-phase B (99.9:0.1 vol/vol methanol/acetic acid) over 1 min, a linear gradient to 100% mobile phase B over 12 min, and then 10 min at 100% mobile-phase B. MS analyses were carried out using electrospray ionization and Q1 scans in the positive ion mode. Ion spray voltage was 5.0 kV and source temperature was 450 °C. For each method, internal standard peak areas were monitored for quality control and individual samples with peak areas differing from the group by more than two SDs were reanalyzed. MultiQuant software (version 1.2; AB Sciex) was used for automated peak integration and metabolite peaks were manually reviewed for quality of integration and compared against a known standard to confirm identity.

Microarray Analysis. RNA was isolated by TRIzol extraction according to manufacturer instructions (Invitrogen), purified using the RNeasy Mini kit (Qiagen), and hybridized on Affymetrix Mouse Genome 430 2.0 GeneChip by the Biopolymers facility at Harvard Medical School. Affymetrix DAT files were processed using the Affymetrix Gene Chip Operating System to create .cel files that were further analyzed using GenePattern software (1). Expression datasets were created using the dChip algorithm. Gene set enrichment analysis (GSEA) was performed using the MSigDB c5 Gene Ontology biological processes gene sets (2). Enrichment scores depicted in Fig. 3 *B* and *C* are calculated as previously described (2). Briefly, in Fig. 3*B*, the *x* axis represents all genes on the microarray, ranked from most correlated with the FLOX animals (*Left*) to most correlated with the MKO animals (*Right*). In Fig. 3*C*, the *x* axis represents the genes in the microarray ranked from most correlated with the control diet (*Left*) to the most correlated with the CR diet (*Right*). In Fig. 3 both *B* and *C*, the enrichment score (*y* axis) represents the relative distribution of the subset of genes that are in the mitochondrial pathway. Mitochondrial genes cluster near FLOX relative to MKO (Fig. 3*B*) and near CR relative to C (Fig. 3*C*).

Quantitative Real-Time PCR. RNA was isolated from tissues as described above. cDNA was synthesized using the iScript cDNA synthesis kit (BioRad) and subjected to quantitative real-time PCR using Syber Green I Mastermix on a Lightcycler 480 (Roche). Each value was normalized to an internal reference gene, beta-2-microglobulin. Primer sequences used for real-time PCR are as follows: *Ldha* forward, 5′-AGGCTCCCCAGAACAAGATT-3′ and reverse, 5′-TCTCGCCCTTGAGTTTGTCT-3′; *Idh2* forward, 5′-CGCCCATGGCGACCAGTACA-3′ and reverse, 5′-CAACGCCTCCGGCAGGGAAG-3′; *Sdha* forward, 5′-ATGACACTGTGAAAGGCTCCGACT-3′ and reverse, 5′-TTCCCAAACTTGAGGCTCTGTCCA-3′; *Fh* forward, 5′-TGCATATTGCTGCTGCAGTGGAAG-3′ and reverse, 5′-ACCATCGCATACTGGACTTGCTGA-3′; *Mdh2* forward, 5′-GGCCAAGGCTGGAGCAGGTTC-3′ and reverse, 5′-TCATGGCGTCCACGAGGGAGA-3′; *Tfam* forward, 5′-ATGTCTCCGGATCGTTTCAC-3′ and reverse, 5′-CCAAAAAGACCTCGTTCAGC-3′; *Cycs* forward, 5′-GCAAGCATAAGACTGGACCAAA-3′ and reverse, 5′-TTGTTGGCATCTGTGTAAGAGAATC-3′; *Atp5o* forward, 5′-AGGCCCTTTGCCAAGCTT-3′ and reverse, 5′-TTCTCCTTAGATGCAGCAGAGTACA-3′; *Mcad* forward, 5′-AGGGTTTAGTTTTGAGTTGACGG-3′ and reverse, 5′-CCCCGCTTTTGTCATATTCCG-3′; *Aco1* forward, 5′-TTCGGGCCAGGAGTGGCTCA-3′ and reverse, 5′-CTTCCTCGCGGCCTGTCTGC-3′; *Cpt1b* forward, 5′-GGATGTTCGAGATGCACAGC-3′ and reverse, 5′-GGAAGCTGTAGAGCATGGGCCG-3′; *Sod1* forward, 5′-TGAGGTCCTGCACTGGTAC-3′ and reverse, 5′-CAAGCGGTGAACCAGTTGTG-3′; *Sod2* forward, 5′-ATCTGTAAGCGACCTTGCTC-3′ and reverse, 5′-GCCTGCACTGAAGTTCAATG-3′; *Gpx1* forward, 5′-AGTCCACCGTGTATGCCTTCT-3′ and reverse, 5′-GAGACGCGACATTCTCAATGA-3′; *Gpx3* forward, 5′-TGGCTTGGTCATTCTGGGC-3′ and reverse, 5′-CCCACCTGGTCGAACATACTT-3′; *Prdx3* forward, 5′-GGTTGCTCGTCATGCAAGTG-3′ and reverse, 5′-CCACAGTATGTCTGTCAAACAGG-3′; *Prdx5* forward, 5′-CCGGAAAGAAGCAGGTTGG-3′ and reverse, 5′-GGCATCTCCCACCTTGATCG-3′; *Pgc1b* forward, 5′-AGAT-

GAAGATCCAAGCTGCCCACA-3′ and reverse, 5′-TCCTCCTCCATTGGCTTGTATGGA-3′; *Pgc1a* forward, 5′-AGCCGTGACCACTGACAACGAG-3′ and reverse, 5′-GCTGCATGGTTCTGAGTGCTAAG-3′ and *B2m* forward, 5′-AGATGAGTATGCCTGCCGTGTGAA-3′ and reverse, 5′-TGCTGCTTACATGTCTCGATCCCA-3′.

Western Blotting. Skeletal muscle was homogenized in ice-cold RIPA buffer and protein content was determined using the BCA Protein Assay kit (Pierce). The following antibodies were used for immunoblotting: tubulin (Sigma) and Total OXPHOS Rodent Antibody mixture (Mitosciences).

Electron Microscopy. Microscopy was performed on red and white muscle fibers of the tibialis anterior and extensor digitorum longus (TA/EDL) muscles. Tissues were immersion fixed in 2.5% glutaraldehyde, 2% paraformaldehyde, in 0.1 M cacodylate buffer pH 7.4 (modified Karnovsky's fixative) for at least 1 h at room temperature. Tissues were washed four times for 10 min each in 0.1 M cacodylate buffer, fixed secondarily in 1% osmium tetroxide in buffer for 1 h at 4 °C, and then washed four times for 10 min in deionized water before being immersed in 2% aqueous uranyl acetate to be contrast fixed overnight at 4 °C. The following day the tissues were washed four times for 10 min in deionized water, then taken through a dehydration series including 30, 50, 70, 95, and 100% ethanol for 10 min each at 4 °C. Tissues were dehydrated at room temperature with 100% ethanol three times for 10 min each and 100% propylene oxide two times for 15 min each. Infiltration proceeded overnight with 1:1 propylene oxide and LX112 Epon resin. Propylene oxide was evaporated before removing the remaining resin and adding 100% freshly made resin for overnight incubation. Samples were placed in a vacuum oven at 60 °C for 2 h and embedded in flat molds and cured at 60 °C over 48 h. Cured blocks were sectioned using a Leica Ultracut E ultramicrotome with a diamond knife set to cut sections at 80 nm thickness that were put on 2 mm × 0.5 mm formvar-coated copper slot grids that had been carbon coated and glow discharged. Grids were contrast stained with 2% uranyl acetate for 10 min and lead citrate for 5 min. Grids were imaged on a JEOL 1400 transmission electron microscope equipped with a side mount Gatan Orius SC1000 digital camera. Mitochondrial density was calculated by measuring the total area covered by mitochondria relative to total fiber area using ImageJ software (National Institutes of Health).

Enzyme Activity Assays. Muscle samples were homogenized in buffer (saccharose 280 mM, Tris 10 mM, pH 7.4) and the mitochondrial-enriched fraction was collected by centrifugation (650 × *g* for 20 min at 4 °C). Complex I, complex IV, citrate synthase (CS), and lactate dehydrogenase (LDH) activity were measured spectrophotometrically as previously described (3). Briefly, complex I (NADH ubiquinone reductase) activity was measured by monitoring the oxidation of NADH at 340 nm. Complex IV (cytochrome *c* oxidase) activity was determined by monitoring the oxidation of reduced cytochrome *c* at 550 nm. Citrate synthase activity was measured by monitoring the change in optical density of 5,5′-dithio-bis(2-nitrobenzoic acid) at 412 nm. Lactate dehydrogenase activity was determined by monitoring the oxidation of NADH at 340 nm in the presence of pyruvate. Activities were normalized to protein content and expressed as nmol/min/mg protein.

1. Reich M, et al. (2006) GenePattern 2.0. *Nat Genet* 38:500–501.
2. Subramanian A, et al. (2005) Gene set enrichment analysis: A knowledge-based approach for interpreting genome-wide expression profiles. *Proc Natl Acad Sci USA* 102:15545–15550.
3. Flamment M, et al. (2009) Effects of the cannabinoid CB1 antagonist, rimonabant, on hepatic mitochondrial function in rats fed a high fat diet. *Am J Physiol Endocrinol Metab*, 10. 1152/ajpendo. 00169. 2009.

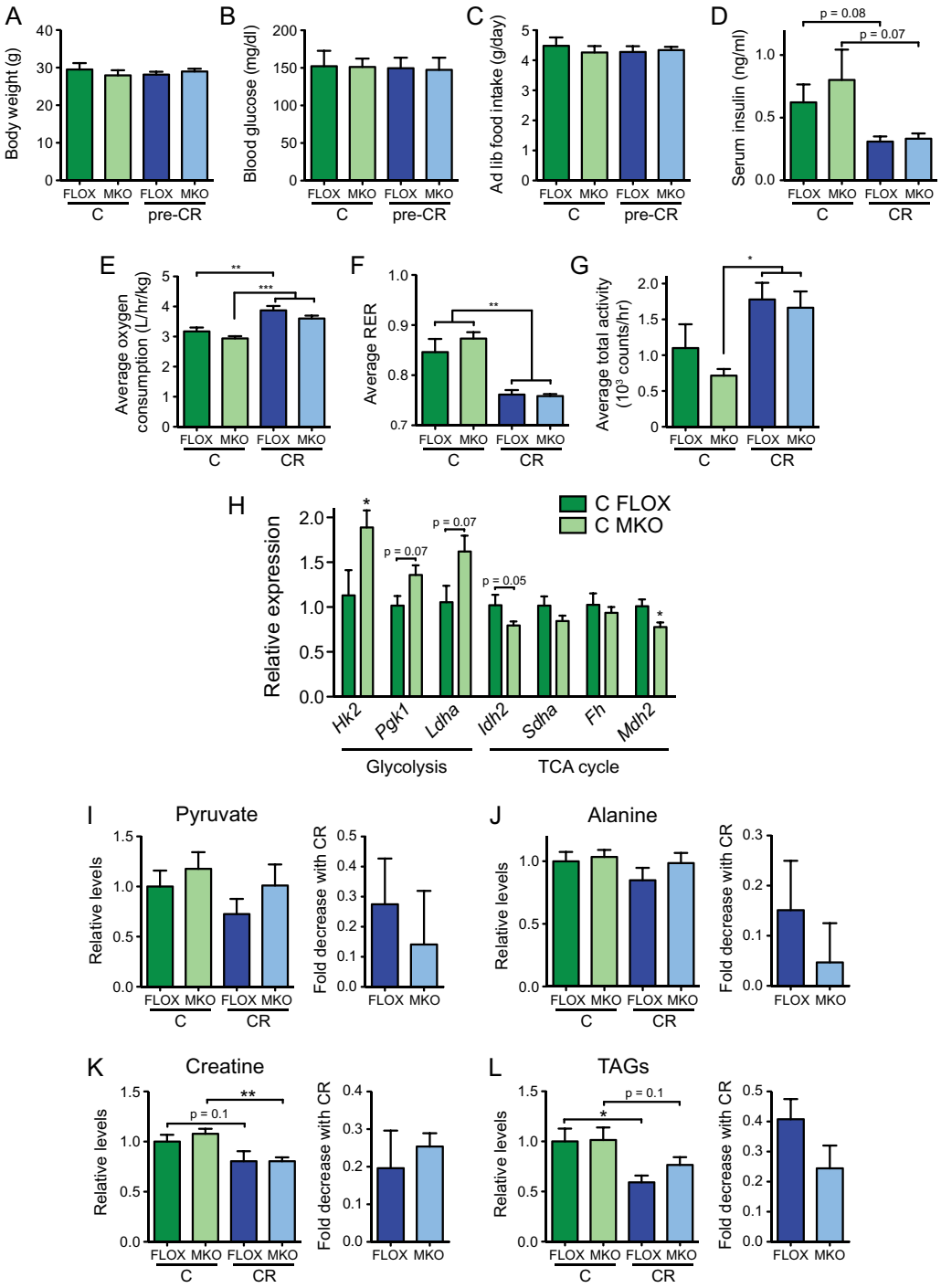

Fig. S1. FLOX and MKO mice have similar metabolic responses to calorie restriction (CR). (*A–C*) At the start of the experiment, all four groups of mice [FLOX control (C), MKO C, FLOX CR, and MKO CR] had equivalent body weight (*A*), resting blood glucose (*B*), and ad libitum food intake (*C*), indicating that all four groups had the same starting point before initiation of CR. (*D*) CR reduces serum insulin levels in both FLOX and MKO mice. (*E–G*) CR mice have higher average oxygen consumption (*E*), fatty acid oxidation (as measured by the respiratory exchange ratio, RER) (*F*), and total activity (*G*) during the light phase (7:00 AM–7:00 PM). Significance was assessed by two-way ANOVA followed by Bonferroni posttest. (*H*) RNA was isolated from the TA/EDL muscles of FLOX and MKO mice on a control diet and expression of genes involved in glycolysis and the tricarboxylic acid (TCA) cycle were measured by qRT-PCR. (*I–L*) Metabolite levels were measured by LC/MS in serum from FLOX and MKO mice on control or CR diets. Pyruvate (*I*) and alanine (*J*) are slightly reduced by CR in FLOX mice. CR reduced creatine (*K*), a marker of mitochondrial dysfunction, and total trigylcerides (TAGs) (*L*). Fold decrease with CR represents the fold change with CR relative to control mice of the same genotype. All experiments were performed on two independent cohorts of mice. Both cohorts showed equivalent results. (*A–C* and *E–H*) All results shown are from a single cohort, $n = 4–8$; (*D* and *I–L*) data from both cohorts were pooled, $n = 9–16$ per group. All bars, SEM. *P* value calculated by Student's *t* test unless otherwise indicated. $*P < 0.05$, $**P < 0.01$, $***P < 0.001$ unless otherwise noted.

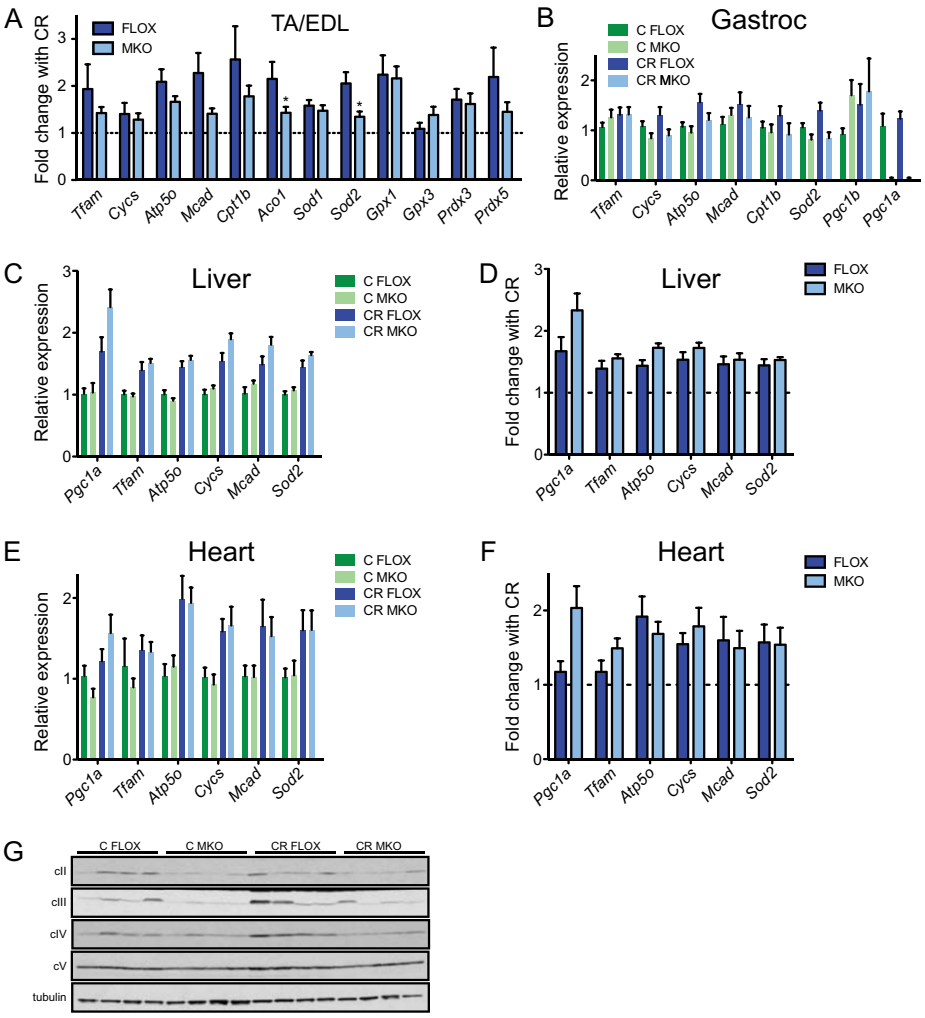

Fig. S2. Skeletal muscle PGC-1α is required for the full induction of mitochondrial genes during CR. (*A*) Expression of mitochondrial genes in TA/EDL muscles was measured by qRT-PCR. Mitochondrial gene induction was calculated as the fold change in expression of CR mice relative to control mice of the same genotype. The data demonstrate that CR induces expression of several genes through PGC-1α, but that some genes can be induced even in the absence of PGC-1α. (*B*) qRT-PCR of RNA from gastrocnemius demonstrates that CR induces expression of several genes through PGC-1α, but that some genes can be induced even in the absence of PGC-1α. (*C* and *E*) Mitochondrial gene expression was measured by qRT-PCR in liver (*C*) and heart (*E*) of FLOX and MKO mice on control and CR diets. (*D* and *F*) The fold change in gene expression with CR in liver (*D*) and heart (*F*) illustrates that both FLOX and MKO mice have similar increases in expression of mitochondrial genes during CR. (*G*) Levels of oxidative phosphorylation (OXPHOS) complexes were measured using Western blots of gastrocnemius muscle from control and CR FLOX and MKO mice. Antibodies used were against representative subunits of OXPHOS complexes II–V and tubulin was used to show equal loading of protein lysates. Bars, SEM; n = 4–8. Where indicated, significance is assessed by Student's t test, $^*P < 0.05$.

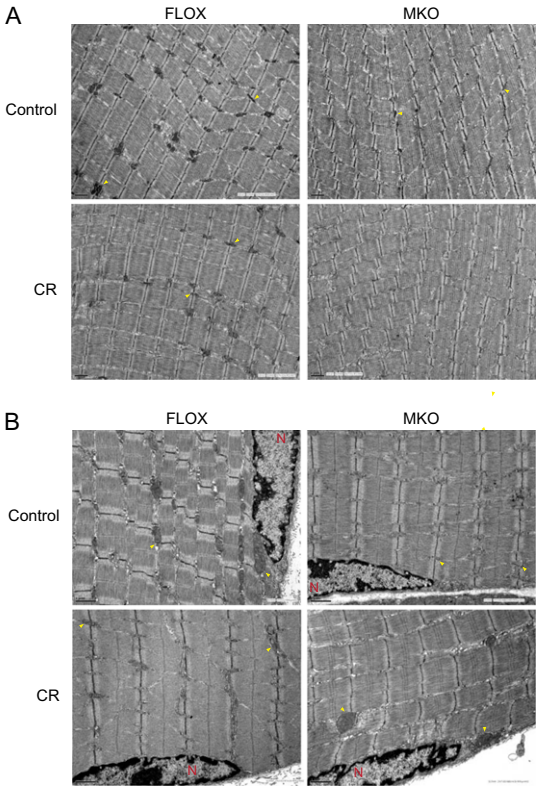

Fig. S3. Representative EM images of the center (*A*) and periphery (*B*) of white (glycolytic) muscle fibers from TA/EDL of control or CR FLOX and MKO mice. Arrowheads indicate representative mitochondria. N, nucleus. (Scale bar, 1 μm.)

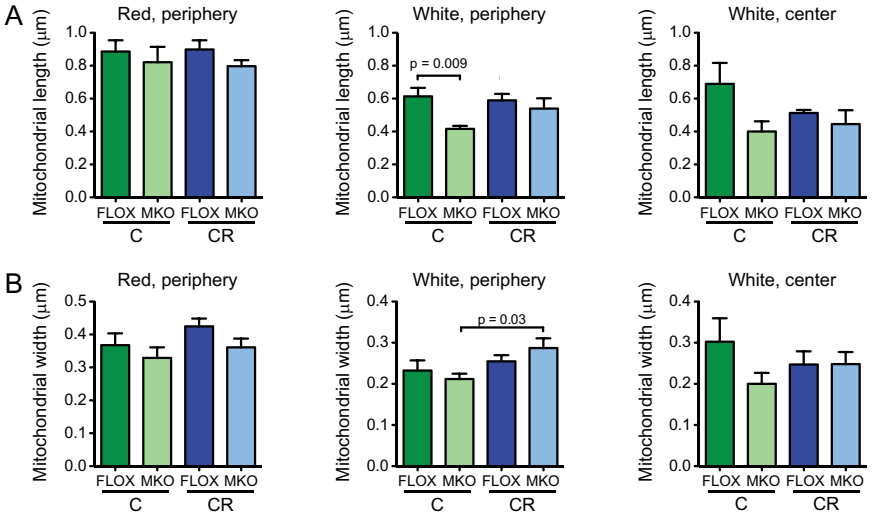

Fig. S4. Summary of the influence of CR on mitochondrial size. (*A*) Average mitochondrial length and (*B*) average mitochondrial width were measured in both red and white muscle fibers from the TA/EDL muscles of FLOX and MKO mice on control or CR diets. EM images were taken from both the center of the myofiber and the periphery, and these regions were analyzed separately. Three separate fibers were imaged from each mouse, and three to four mice per group were analyzed. All bars, SEM. Significance was assessed by Student's *t* test.

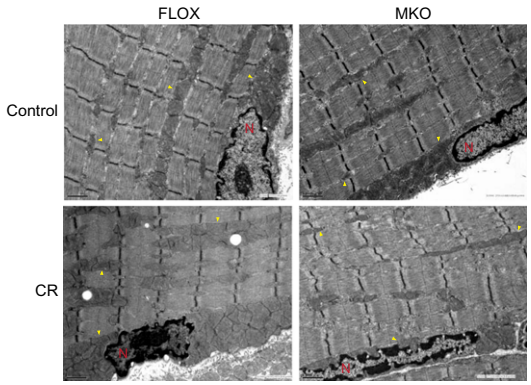

Fig. S5. Representative EM images of the periphery of red (oxidative) muscle fibers from TA/EDL of control or CR FLOX and MKO mice. Arrowheads indicate representative mitochondria. N, nucleus. (Scale bar, 1 μm.)

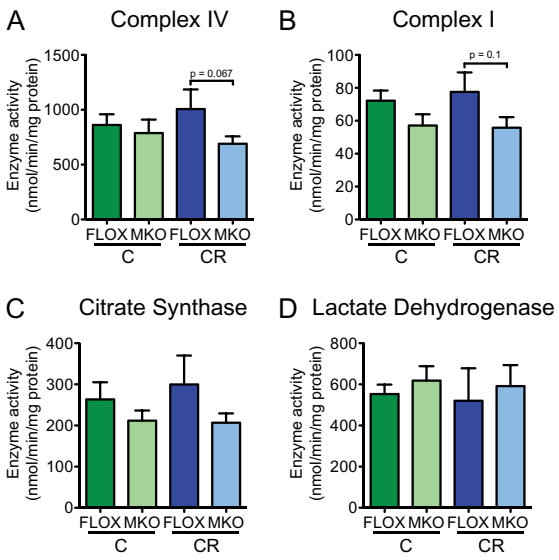

Fig. S6. Metabolic enzyme activities. (*A*–*D*) Metabolic activities were measured in homogenized quadriceps muscle from FLOX and MKO mice on control and CR diets and normalized to protein content. (*A*) Mitochondrial electron transport chain complex IV (cytochrome *c* oxidase), (*B*) mitochondrial electron transport chain complex I (NADH ubiquinone reductase), and (*C*) citrate synthase, the rate limiting step of the TCA cycle, all have a trend of increased activity in CR FLOX mice. In contrast, CR MKO mice do not show an increase in oxidative capacity. (*D*) Activity of cytoplasmic lactate dehydrogenase does not increase with CR. Bars, SEM; n = 4–8. Where indicated, significance is assessed by Student's t test.

Table S1. GSEA analysis reveals Gene Ontology biological processes enriched by CR in FLOX mice

Gene set	Size	NES	*P* value	Max rank
COFACTOR_METABOLIC_PROCESS	49	−1.58	0.006	2,608
CELLULAR_BIOSYNTHETIC_PROCESS	259	−1.39	0.015	3,107
REGULATION_OF_CELL_GROWTH	38	−1.45	0.016	3,216
COENZYME_METABOLIC_PROCESS	35	−1.55	0.017	1,921
CARBOHYDRATE_METABOLIC_PROCESS	154	−1.38	0.021	4,397
LIPID_CATABOLIC_PROCESS	31	−1.48	0.031	3,965
BIOSYNTHETIC_PROCESS	388	−1.24	0.038	3,161
CELLULAR_CARBOHYDRATE_METABOLIC_PROCESS	107	−1.34	0.06	5,144
ELECTRON_TRANSPORT_GO_0006118	41	−1.32	0.067	4,657
RESPONSE_TO_ABIOTIC_STIMULUS	79	−1.33	0.09	4,783
REGULATION_OF_GROWTH	48	−1.32	0.094	3,216
RNA_PROCESSING	132	−1.35	0.098	2,866

GSEA, gene set enrichment analysis; size, number of genes in set; NES, normalized enrichment score.

Table S2. GSEA analysis reveals Gene Ontology biological processes enriched by CR in MKO mice

Gene set	Size	NES	*P* value	Max rank
DNA_DEPENDENT_DNA_REPLICATION	46	−1.54	0.006	3,258
CELLULAR_BIOSYNTHETIC_PROCESS	259	−1.59	0.008	2,824
DNA_REPLICATION	85	−1.52	0.008	3,319
BIOSYNTHETIC_PROCESS	388	−1.38	0.01	2,824
RNA_PROCESSING	132	−1.56	0.014	4,090
TRANSLATION	137	−1.68	0.02	2,950
MRNA_PROCESSING_GO_0006397	59	−1.61	0.023	2,158
HOMEOSTATIC_PROCESS	179	−1.29	0.024	1,546
COENZYME_METABOLIC_PROCESS	35	−1.55	0.033	1,149
MACROMOLECULE_BIOSYNTHETIC_PROCESS	259	−1.4	0.033	2,950
RNA_SPLICING	68	−1.46	0.034	4,090
COFACTOR_METABOLIC_PROCESS	49	−1.52	0.035	3,068
NEGATIVE_REGULATION_OF_CELLULAR_PROTEIN_METABOLIC_PROCESS	39	−1.32	0.039	2,187
DNA_METABOLIC_PROCESS	224	−1.29	0.043	3,319
NUCLEOTIDE_METABOLIC_PROCESS	36	−1.46	0.047	1,954
DNA_REPAIR	111	−1.27	0.082	3,293
MRNA_METABOLIC_PROCESS	69	−1.4	0.091	2158

GSEA, gene set enrichment analysis; size, number of genes in set; NES, normalized enrichment score.

Other Supporting Information Files

Dataset S1 (XLS)